

## **Distribution Agreement**

In presenting this thesis as a partial fulfillment of the requirements for a degree from Emory University, I hereby grant to Emory University and its agents the non-exclusive license to archive, make accessible, and display my thesis in whole or in part in all forms of media, now or hereafter now, including display on the World Wide Web. I understand that I may select some access restrictions as part of the online submission of this thesis. I retain all ownership rights to the copyright of the thesis. I also retain the right to use in future works (such as articles or books) all or part of this thesis.

Nicholas Keung

April 10, 2023

Preparation and Structural Analysis of the Human Respiratory Syncytial Virus M2-2 Protein

by

Nicholas Keung

Bo Liang  
Adviser

Biology

Bo Liang  
Adviser

William Kelly  
Committee Member

Kate McKnelly  
Committee Member

2023

Preparation and Structural Analysis of the Human Respiratory Syncytial Virus M2-2 Protein

By

Nicholas Keung

Bo Liang

Adviser

An abstract of  
a thesis submitted to the Faculty of Emory College of Arts and Sciences  
of Emory University in partial fulfillment  
of the requirements of the degree of  
Bachelor of Science with Honors

Biology

2023

## Abstract

### Preparation and Structural Analysis of the Human Respiratory Syncytial Virus M2-2 Protein By Nicholas Keung

The human respiratory syncytial virus (hRSV) is a non-segmented negative strand (NNS) RNA virus that leads to respiratory infection, particularly in infants and the elderly. Despite its heavy public health burden, an efficient vaccine has not yet been developed. The viral genome is encapsidated by the nucleoprotein N, RNA polymerase L, and cofactors P and M2-1 to form the helical ribonucleocapsid. The M2-2 protein, encoded by the second open reading frame (ORF) of the M2 gene, is responsible for ribonucleocapsid rearrangement and for favoring viral replication over transcription. While many of the structural studies on RSV proteins have been on the G and F membrane proteins and the ribonucleocapsid proteins, there is no structural data on M2-2.

To better understand the function of M2-2 and the mechanism behind its activity, we demonstrate the expression and purification of M2-2 and maltose-binding protein (MBP)-tagged M2-2. We report MBP-M2-2 expression in *E. coli* competent cells, and using affinity chromatography, ion exchange, and size exclusion chromatography, we were able to obtain pure samples of both proteins. We also describe sitting-drop and hanging-drop vapor diffusion crystallization experiments which show growth of microcrystals. Finally, we used dynamic light scattering and negative stain electron microscopy to characterize purified M2-2 and MBP-M2-2. This data takes the first step toward solving the structure of M2-2. Structural data on M2-2 will reveal its function at a biochemical level, deepening our understanding of viral RNA synthesis and providing an avenue for vaccine development.

Preparation and Structural Analysis of the Human Respiratory Syncytial Virus M2-2 Protein

By

Nicholas Keung

Bo Liang

Adviser

A thesis submitted to the Faculty of Emory College of Arts and Sciences  
of Emory University in partial fulfillment  
of the requirements of the degree of  
Bachelor of Science with Honors

Biology

2023

## Acknowledgements

I would like to thank my Principle Investigator Dr. Bo Liang for giving me the opportunity to do research in his laboratory for the past two and a half years. I appreciate his patience and support throughout my time. He introduced me to the field of biochemistry and structural biology, and I learned a lot through his guidance. I would also like to thank Dr. Zhenhang Chen for being my mentor and for teaching me everything I know now. I am extremely grateful for his constant support and willingness to help. I want to thank Dylan Blohm, Eliseo Salas, and the other members of the Liang Laboratory for their help and encouragement along the way.

In addition, I would like to thank the other members of my honor thesis committee, Dr. William Kelly and Dr. Kate McKnelly, for dedicating their time, advice, and support throughout this project.

## Table of Contents

<b>Introduction .....</b>	<b>1</b>
<b>Results .....</b>	<b>4</b>
Expression and Purification of MBP-M2-2 .....	4
Purification of Untagged M2-2.....	8
MBP-M2-2 Crystal Screen and Optimization.....	11
DLS and Negative Stain EM of M2-2 and MBP-M2-2 .....	13
<b>Methods and Materials .....</b>	<b>16</b>
<i>E. coli</i> Transformation and MBP-M2-2 Expression.....	16
MBP-M2-2 Purification.....	17
M2-2 Purification .....	18
Crystal Screening and Optimization .....	19
Dynamic Light Scattering.....	20
Negative Stain Electron Microscopy .....	20
<b>Discussion and Future Directions.....</b>	<b>21</b>
<b>Supplementary Figures.....</b>	<b>24</b>
<b>References .....</b>	<b>28</b>

## Figures

1. The 3'-5' negative-sense RSV genome .....	3
2. MBP-fused M2-2 gene insert in pET expression vector .....	5
3. MBP-tagged M2-2 Purification.....	7
4. Untagged M2-2 Purification.....	10
5. MBP-M2-2 Crystal Screen Microcrystal Growth .....	12
6. MBP-M2-2 Crystal Optimization Experiments .....	14
7. DLS Analysis of M2-2, MBP-M2-2 <sub>P1</sub> , and MBP-M2-2 <sub>P2</sub> .....	15
8. Negative Stain EM of M2-2 and MBP-M2-2 <sub>P1</sub> .....	16
9. TEV Protease Digestion Experiment.....	24
10. M2-2 Purification Optimization Experiment .....	25
11. Crystal Optimization Conditions.....	26
12. M2-2 Subcloning .....	27

## INTRODUCTION

Respiratory syncytial virus (RSV) infection predominantly infects the upper and lower respiratory tract of patients, many of whom are infants, the elderly, or immunocompromised patients (Collins et al. 2013). The virus primarily targets ciliated epithelial cells in the trachea, bronchi, and bronchioles (Collins et al. 2013). RSV has been estimated to cause over 3.4 million hospitalization and 95,000-150,000 global deaths (Boyoglu-Barnum et al. 2019). Specifically in the United States, RSV is estimated to cause 14,000 deaths every year in adults, and recent outbreaks have prompted a healthcare emergency (Boyoglu-Barnum et al. 2019). Symptoms can manifest as a minor cold, but they can be severely worsened with other comorbidities such as premature birth, old age, heart disease, or lung disease in infant and geriatric patients (Collins et al. 2013). In severe cases, lower respiratory tract infection by RSV has been shown to cause other chronic conditions such as asthma, chronic bronchitis, and obstructive pulmonary disease (Griffiths et al. 2017). Despite the high disease burden caused by RSV, an efficient vaccine has not been developed for over 60 years.

In the 1960s, the formalin-inactivated whole-virus (FI-RSV) vaccine was developed. This vaccine was administered to a small cohort of infants who did not experience adverse reactions prior to natural RSV infection. However, upon infection with natural RSV, the vaccinated infants experienced more aggressive symptoms compared to unvaccinated infants, leading to enhanced RSV disease (ERD). Development of ERD after the FI-RSV vaccine is specific to RSV-naïve patients and has now been corroborated in mouse models. Other animal studies have found that ERD occurs with protein-based vaccines, such as the whole inactivated virus, but it does not occur with natural RSV infection (Collins et al. 2013). The risk of ERD, difficulty in

inducing immunity, and the young age of most patients make vaccine development difficult. However, there are several live attenuated RSV vaccines and subunit vaccines under development that show promise. In particular, the RSV prefusion F protein-based (RSVpreF) vaccine administered to mothers successfully produced neutralizing antibodies in significantly higher titers in infant umbilical cord blood (Simões et al. 2022). The vaccine is currently under phase III clinical trials and is under review by the FDA.

RSV is a non-segmented negative strand (NNS) RNA virus, with its genome containing 10 genes that encode for 11 proteins (Figure 1). The M2 gene contains two open reading frames (ORFs) that produce M2-1 and M2-2. Glycoprotein, G, and the fusion glycoprotein, F, are surface proteins responsible for host cell binding and membrane fusion, respectively (Battles and McLellan 2019). The RSV ribonucleocapsid consists of the RNA genome encapsidated by the nucleoprotein, N, along with the large RNA-dependent RNA polymerase, L, its phosphoprotein cofactor, P, and the transcription elongation factor, M2-1 (Blanchard et al. 2020). After the viral membrane fuses with the host cell, the ribonucleocapsid serves as a template for primary transcription by the pre-formed polymerases (Collins et al. 2013). As viral proteins accumulate, the newly synthesized N and P proteins then allow for RNA replication, producing full-length antigenomes and genomes (Collins et al. 2013). The genomic RNAs then allow for secondary transcription and further replication (Blanchard et al. 2020). After 8 hours post-infection (hpi), spherical inclusion bodies (IBs) are found in the cytoplasm consisting of nucleocapsids with N, P, L, and M2-1 (Rincheval et al. 2017). These IBs have properties of liquid organelles and have been shown to synthesize new viral RNA, confirming their roles as viral factories (Nikolic et al. 2017; Rincheval et al. 2017).

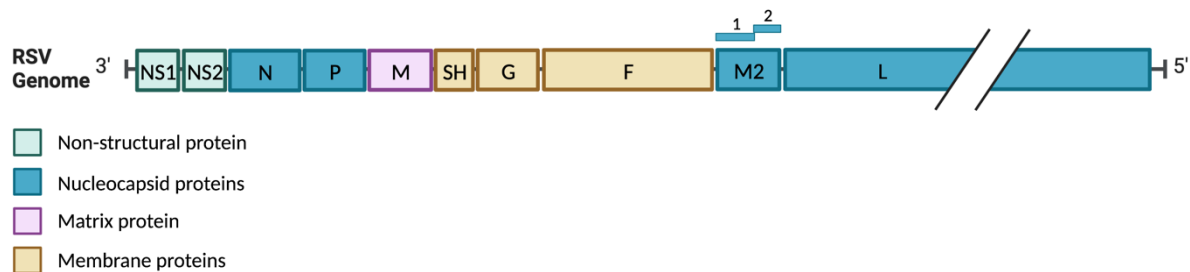


**Figure 1. The 3'-5' negative-sense RSV genome.** The RSV genome, created with BioRender.com, encodes a total of 11 proteins with overlapping ORFs in the M2 gene.

Published research on M2-2 has been limited, but it has been shown to function as a regulatory factor mediating RNA synthesis. Deletion of M2-2 has been shown to decrease RNA replication in favor of transcription. Minigenome assays have shown that increasing amounts of M2-2 progressively reduce expression while the loss of M2-2 shows a decrease in genomic and antigenomic RNA (Bermingham and Collins 1999). This transcription inhibition by M2-2 has been shown to require P protein phosphorylation (Asenjo and Villanueva 2016). However, overexpression of M2-2 led to inhibition of RNA replication, suggesting that RNA synthesis inhibition is not specific (Cheng et al. 2005). Notably, transfection of M2-2 mRNA at 10 hpi did not have a noticeable effect on infection, indicating a time window for M2-2 control (Blanchard et al. 2020). Regardless, M2-2 transfection resulted in decreased interactions between L and N, along with L and genomic RNA (Blanchard et al. 2020). Consequently, after viral infection and primary transcription, accumulation of M2-2 has been proposed to induce ribonucleocapsid rearrangement in favor of replication (Blanchard et al. 2020). In addition to regulating RNA synthesis, a preliminary article also reports that M2-2 may also have a role in inhibiting cellular translation, thus lowering eIF2 $\alpha$  phosphorylation and reducing the formation of stress granules

(Scudero et al. preprint, submitted in 2023). Furthermore, M2-2 serves as a potential target for therapeutics. Viral replication in the mouse respiratory tract was markedly attenuated in M2-2 deletion mutants, and similar results were found in chimpanzee models, highlighting the importance of understanding the function of M2-2 (Jin et al. 2000; Teng et al. 2000).

Structural analysis of RSV and its various proteins is limited, focusing on (1) the surface of the viral membrane, F and G, and (2) the proteins responsible for viral replication—L, P, N, and M2-1. However, currently, there is no reported structural data for M2-2. To address this lack of knowledge, we report the expression of M2-2 bound to maltose-binding protein (MBP) in BL21(DE3) cells, along with the successful purification of MBP-M2-2 and untagged M2-2. In addition, we identified various conditions that promote MBP-M2-2 crystal growth, providing an avenue for X-ray crystallography. Furthermore, we used dynamic light scattering (DLS) and negative stain electron microscopy (EM), finding that M2-2 and MBP-M2-2 appear to form oligomers in solution. Our data offer an initial step towards the unexplored structure of M2-2, which will reveal the biochemical activity of M2-2, deepen our knowledge of the RSV life cycle, and offer a new avenue for RSV therapeutics.

## RESULTS

### Expression and Purification of MBP-M2-2

The M2-2 gene was fused with MBP and a 6x-histidine tag and separated by a TEV protease recognition site. This gene was synthesized by Synbio Technologies in a pET expression vector under the control of a T7 promoter and the *lac* operator (Figure 2). BL21(DE3) *E. coli*

competent cells were then transformed by heat shock and grown to 0.6 OD<sub>600</sub> before inducing expression of MBP-M2-2 (54.9 kDa) with isopropyl  $\beta$ -D-1-thiogalactopyranoside (IPTG).

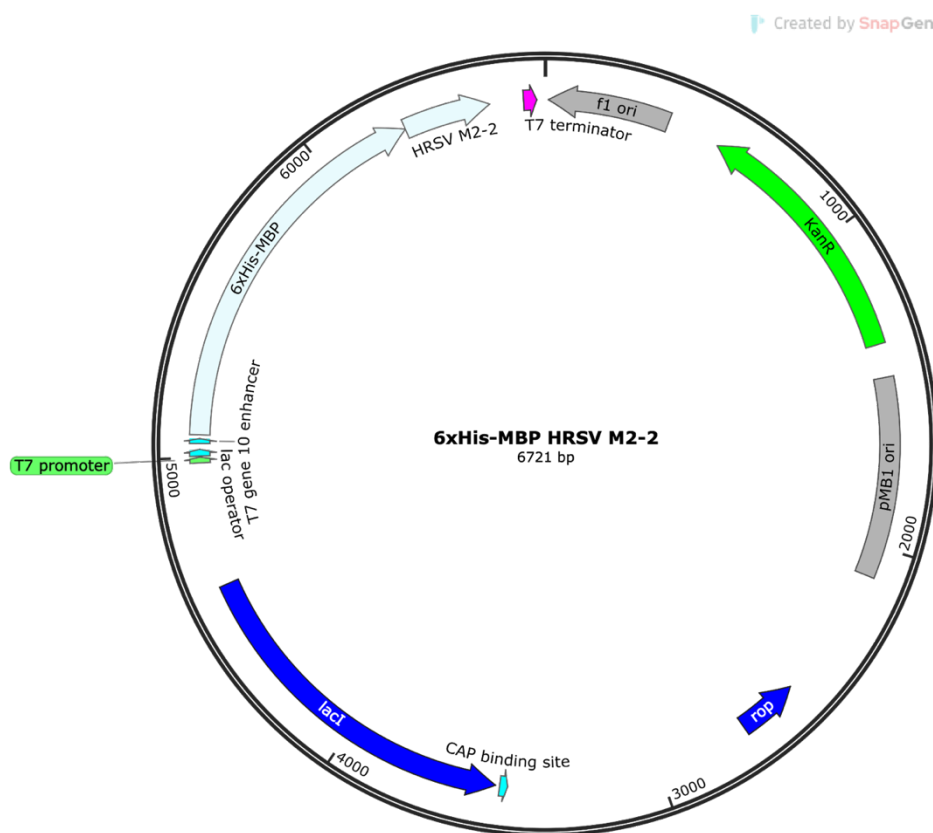


**Figure 2. MBP-fused M2-2 gene insert in pET expression vector.** The M2-2 gene was fused at the N-terminus with a TEV protease recognition site, MBP tag, and a 6x-histidine tag. Gene expression is placed under the control of a T7 promoter and the *lac* operator, as shown using SnapGene® software

The cells were harvested after induction and resuspended in a lysis buffer containing 30 mM Tris-HCl pH 8.0, 300 mM NaCl, 20 mM imidazole. After sonication, the lysate was clarified by centrifugation at 18,000 rpm and incubated overnight with Ni-NTA resin. The sample was then loaded into a gravity column, and the column was washed and eluted with lysis buffer containing imidazole. SDS-PAGE analysis of the elution fractions shows that MBP-tagged M2-2 (MBP-M2-2) is eluted at 20 mM imidazole, suggesting that it may have a low affinity for Ni-NTA

resin (Figure 3a). This trend is consistent despite attempts at increasing the resin volume, increasing the incubation time with the Ni-NTA, and repeatedly loading the lysate on the column. Despite this, the protein also required very high concentrations of imidazole to elute as well. This indicates that although some protein was eluted very early, the protein that remained on the column interacted strongly with the  $\text{Ni}^{2+}$ .

After nickel affinity purification, the fractions containing MBP-M2-2 were pooled, and the sample was dialyzed against a buffer containing 30 mM Tris-HCl pH 8.0, 50 mM NaCl at 4°C overnight. Then, the sample was centrifuged at 12,000 rpm at 4°C for 10 minutes before loading on a 5 mL HiTrap Canto Q ImpRes column. The column was then eluted on an AKTA Pure system with a buffer containing 30 mM Tris-HCl pH 8.0 and an increasing NaCl gradient. Occasionally throughout the purification, NaCl concentration was held constant in order to better separate individual peaks. The initial peak on the chromatogram (19-25 mL) corresponds to the lower molecular weight contaminant proteins (35-50 kDa) while the subsequent larger peak (26-43 mL) contains primarily MBP-M2-2 (Figure 3b-c). The ratio of A260/A280 between peaks 1 and peak 2 was about 0.6, indicating the elution consists of mostly protein. Meanwhile, the A260/A280 ratio in peak 3 (54-59 mL) was approximately 1.9, indicating that the fraction consisted of nucleic acid (Figure 3b). Consequently, anion exchange chromatography was shown to be successful in removing not only contaminant proteins but also nucleic acids from the sample.

The elution fractions from the Q column were finally concentrated to 2 mL and purified using size exclusion chromatography (SEC) on a Superdex 200 Increase 10/300 GL column. The

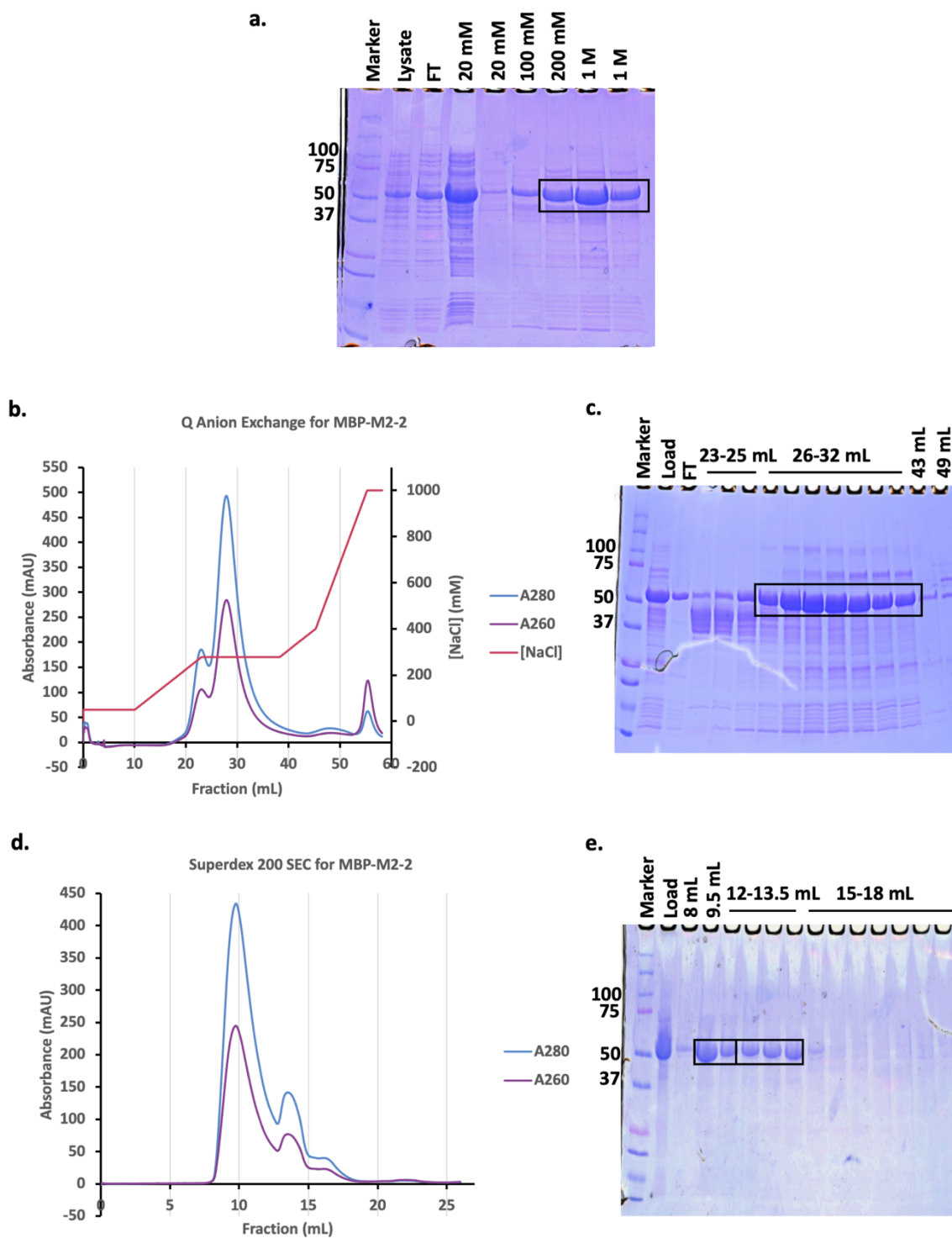


**Figure 3. MBP-tagged M2-2 Purification.** **a** *E. coli* lysate containing MBP-M2-2 was loaded onto Ni-NTA resin. The column was washed, and the protein eluted with lysis buffer containing imidazole. **b** MBP-M2-2 was loaded on a 5 mL HiTrap Capto Q ImpRes column and eluted using a buffer containing 30 mM Tris-

HCl pH 8.0 and a NaCl gradient. The NaCl concentration was intermittently held constant in order to better separate individual peaks. **c** SDS-PAGE analysis of the anion exchange chromatography indicates that the first peak consisted primarily of smaller contaminant proteins while the second peak indicated the elution of MBP-M2-2. **d** MBP-M2-2 was loaded on a Superdex 200 Increase 10/300 GL column and eluted. The chromatogram shows three major peaks. **e** Fractions from SEC were analyzed on SDS-PAGE which revealed bands of purified MBP-M2-2 after SEC.

FPLC chromatogram shows three peaks were eluted (Figure 3d). The fractions were analyzed on SDS-PAGE with the first two peaks (8-12 mL and 12.5-15.5 mL) showing a pure MBP-M2-2 and the third peak (15.5-18 mL) showing no protein (Figure 3e). The fractions were later used for crystallization screening.

### **Purification of Untagged M2-2**

Untagged M2-2 was purified similarly by expressing MBP-M2-2 in *E. coli* and purifying the protein over Ni-NTA resin as described previously. TEV protease was added to the eluted fractions at a 1:20 TEV-to-MBP-M2-2 mass ratio. TEV protease digestion was left for 12 hours in 30 mM Tris-HCl pH 8.0, 300 mM NaCl, 2 mM 2-mercaptoethanol (BME) and then transferred to 30 mM Tris-HCl pH 8.0, 50 mM NaCl for four hours. SDS-PAGE showed that TEV protease successfully digested MBP-M2-2, but some remained (Figure 4a). The sample was loaded onto a Ni-NTA resin gravity column, and the flowthrough was poured through the column additional times to maximize the binding of MBP and TEV protease to the column to separate the untagged M2-2 (11.1 kDa). However, SDS-PAGE analysis of the elutions shows that additional passes through the resin did not significantly increase the binding of MBP or TEV to the column (Figure 4a). Nonetheless, cleaved M2-2 was found in the flowthrough and did not bind to the

column (Figure 4a). The column was then washed with 20 mM imidazole, removing any M2-2 that remained bound to the column, and then eluted with 1 M imidazole.

The cleaved M2-2 was then loaded on a 5 mL HiTrap Capto Q ImpRes column and eluted with 30 mM Tris-HCl pH 8.0 with a NaCl concentration gradient. The ratio of A260 to A280 on the chromatogram showed a large peak (20-36 mL) that was eluted containing protein and a second peak (37-49 mL) that consists of nucleic acid (Figure 4b). The fractions were then run on SDS-PAGE which revealed poor separation of M2-2 from other contaminants, especially MBP (Figure 4c). This could indicate that there is an insufficient difference in charge between M2-2 and the other contaminant proteins. Although the Q column was successful in removing any nucleic acids from the sample, it did not effectively remove any contaminant protein.

Because anion exchange was not as effective as expected, the fractions were pooled and purified over another Ni-NTA column which was able to remove much of the contaminant MBP (Figure 4d). However, the intensity of the M2-2 bands appears significantly reduced, suggesting the loss of protein throughout the steps. The sample was finally loaded on a Superdex 200 10/300 column and eluted as described previously, revealing two large peaks (Figure 4e).

Interestingly, M2-2 was found in the second peak of the chromatogram with very similar values for A280 and A260 (Figure 4e). This could indicate that the eluted protein contained nucleic acid contamination, muddying the ratio of the two absorbance values. In addition, the chromatogram peak was also significantly lower, reaching an A280 maximum of only 62 mAU (Figure 4e). This is indicative of a low volume of protein being detected during elution. The eluted sample was run on SDS-PAGE which showed a purified M2-2 (Figure 4f). Despite successfully purifying the sample, a significant portion of M2-2 was lost through the

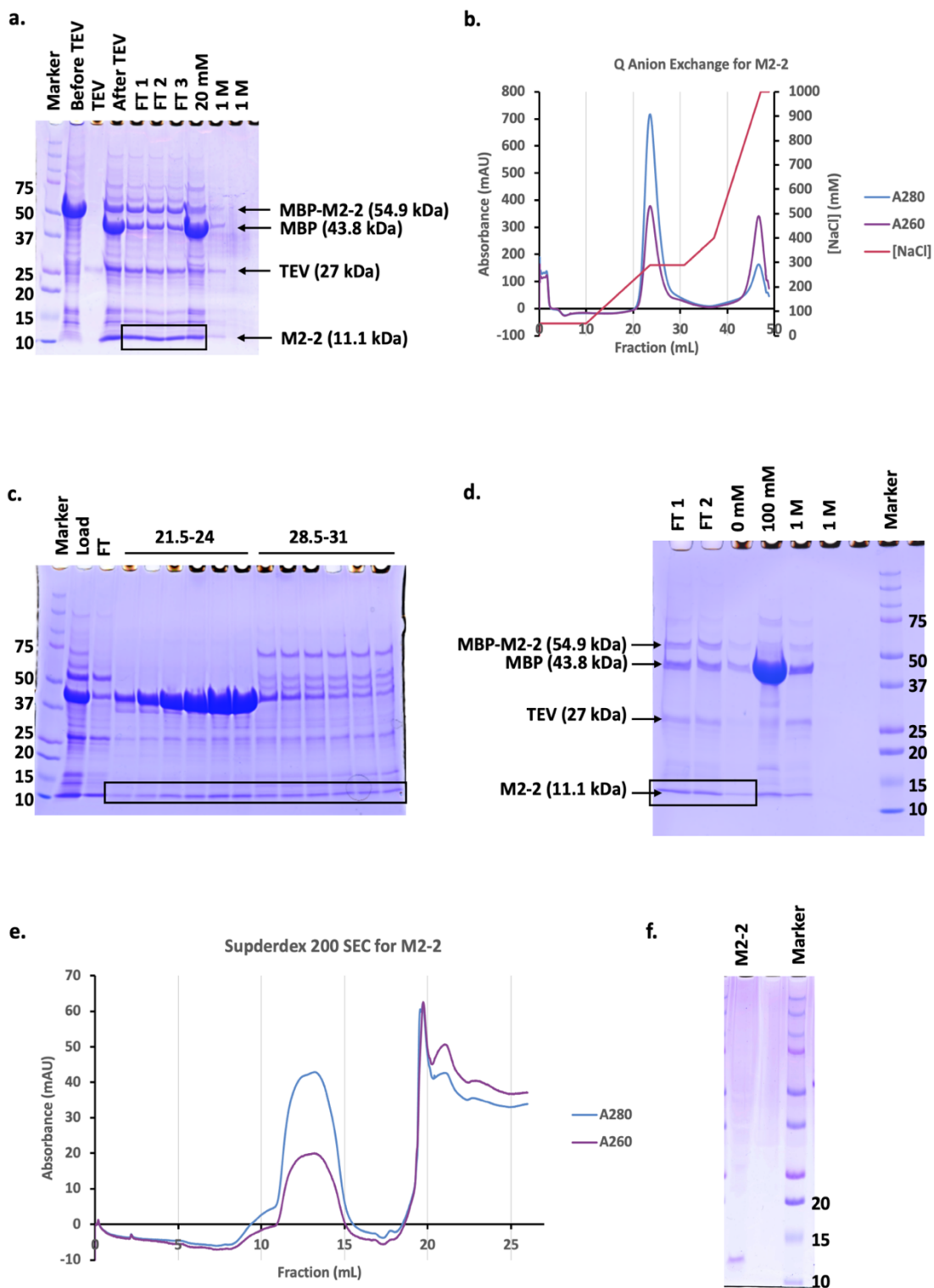


**Figure 4. Untagged M2-2 Purification.** **a** SDS-PAGE shows successful but incomplete TEV protease digestion. The sample was then purified over Ni-NTA resin and washed with imidazole. **b** Cleaved M2-2

was purified by anion exchange chromatography, revealing two major peaks. **c** SDS-PAGE of the anion exchange showed poor separation of M2-2 from contaminant proteins. **d** M2-2 was loaded over an additional Ni-NTA column and eluted with imidazole. **e** M2-2 was further purified by SEC. The chromatogram revealed the elution of two peaks (9-15 mL and 19-23 mL). **f** SDS-PAGE shows that M2-2 was successfully purified.

series of purification attempts with a final yield of 0.048 mg of M2-2 from 12 L of culture.

Purified M2-2 was aliquoted, frozen by liquid nitrogen, and stored at -80°C.

### **MBP-M2-2 Crystal Screen and Optimization**

Purified MBP-M2-2 (Figure 3d-e) was concentrated to 9.93 mg/mL for vapor diffusion crystallization. A Crystal Phoenix (Art Robbins Instruments) was used to set up sitting-drop trays with 768 solution conditions from various crystallization kits (Hampton Research and Rigaku Corporation). Each crystallization drop consisted of 0.2  $\mu$ L of MBP-M2-2 protein (4.97 mg/mL or 9.93 mg/mL) mixed with 0.2  $\mu$ L of solution with 60  $\mu$ L of solution in the reservoir. The trays were then incubated at 30°C and imaged under visible and UV light using a Formulatrix RockImager-1000. Among the conditions tested, three in the Index HT screening kit (Hampton Research) showed crystal-like formations (Figure 5). Imaging these crystals under UV shows fluorescence, suggesting that these formations are made up of protein and ruling out the possibility of salt crystals.

Using the three successful conditions, crystallization was further optimized by adjusting the composition of each condition by 10-20% for a total of 21 conditions on a hanging-drop plate (Supplemental Figure 2). A new sample of MBP-M2-2 was purified by SEC on a Superdex 75 Increase 10/300 GL column (Figure 7a-b). The elutions from the first peak were concentrated

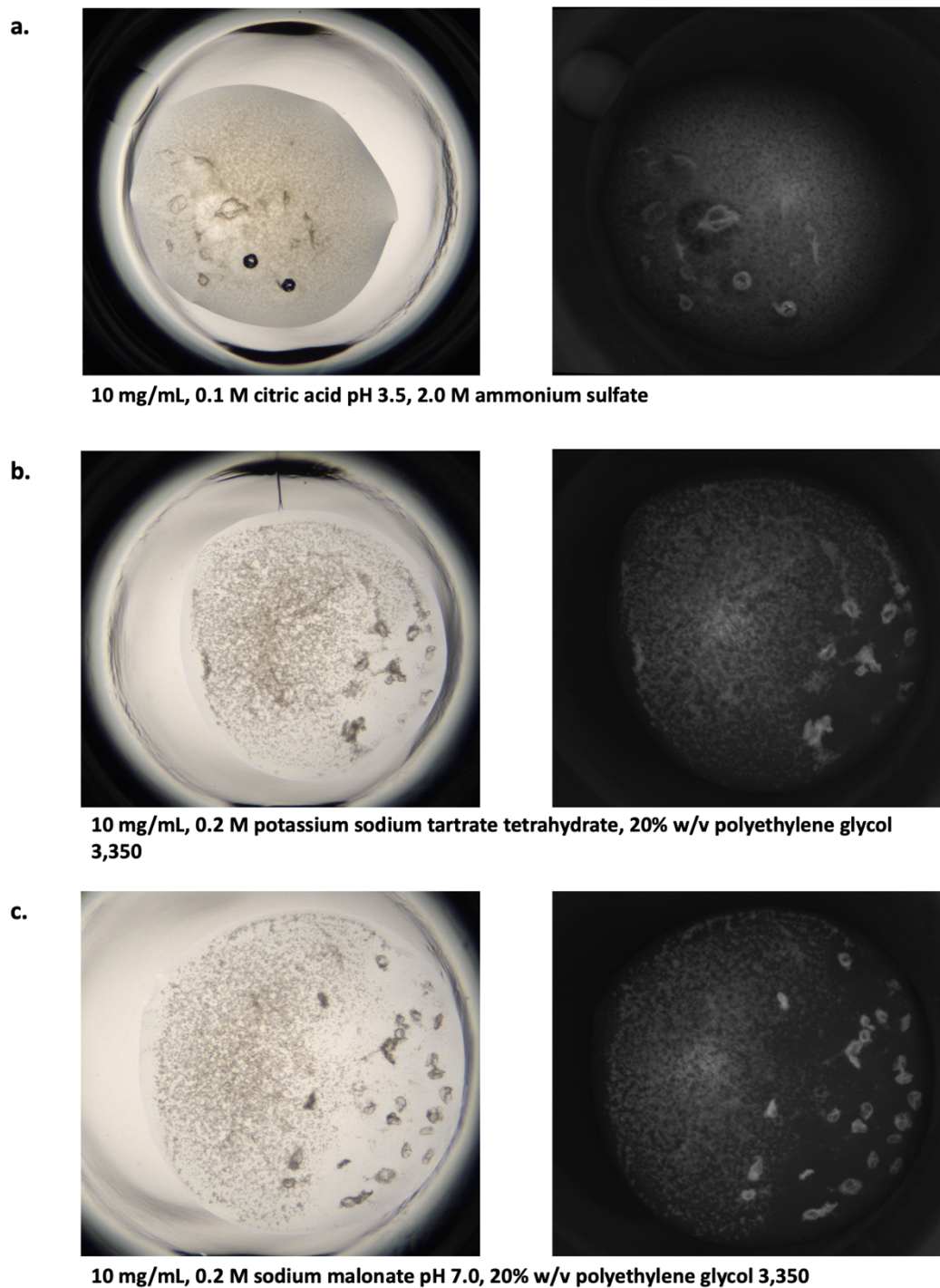


**Figure 5. MBP-M2-2 Crystal Screen Microcrystal Growth.** 768 different sitting-drop crystallization conditions were screened and imaged under visible and UV light. The conditions shown above appear to form microcrystals.

to 2.3 mg/mL based on results from the pre-crystallization test (PCT, Hampton Research) and because precipitation was common in the screening tests at 4.97 and 9.93 mg/mL. Drops consisted of 2  $\mu$ L of MBP-M2-2 (2.3 mg/mL) and 2  $\mu$ L buffer, while 500  $\mu$ L of buffer was used in the reservoir. One condition (100 mM citric acid pH 3.5, 1.8 M ammonium sulfate) appeared to produce a large crystal (Figure 6a). However, given the absence of other crystals and the low pH of the condition, it is most likely a salt crystal. Also, other citric acid conditions did not produce similar crystals. However, two other conditions (170 mM and 180 mM potassium sodium tartrate, 20% polyethylene glycol [PEG] 3350) appear to show the growth of microcrystals (Figure 6b-c).

#### **DLS and Negative Stain EM of M2-2 and MBP-M2-2**

SEC results show that MBP-M2-2 was eluted in two peaks corresponding to different molecular weights (Figure 7a), suggesting that M2-2 has different oligomerization states. Sample from each SEC peak (MBP-M2-2<sub>P1</sub> and MBP-M2-2<sub>P2</sub>) and purified M2-2 (Figure 4f) were loaded on a 384-well plate and imaged using a DynaPro Plate Reader III (Wyatt Technology). Readings show that each sample is homogenous with a calculated radius of 7.7 nm, 8.7 nm, and 5.2 nm for M2-2, MBP-M2-2<sub>P1</sub>, and MBP-M2-2<sub>P2</sub> respectively (Figure 7c). DLS also predicts that the particles in solution have a high molecular weight (160-400 kDa) based on their model. The large radius and high molecular weight seem to suggest that M2-2 and MBP-M2-2 form complexes in solution.

To investigate this further, the sample was imaged using negative stain EM. Samples were loaded on EM grids, washed, and stained with uranyl sulfate. They were then imaged on

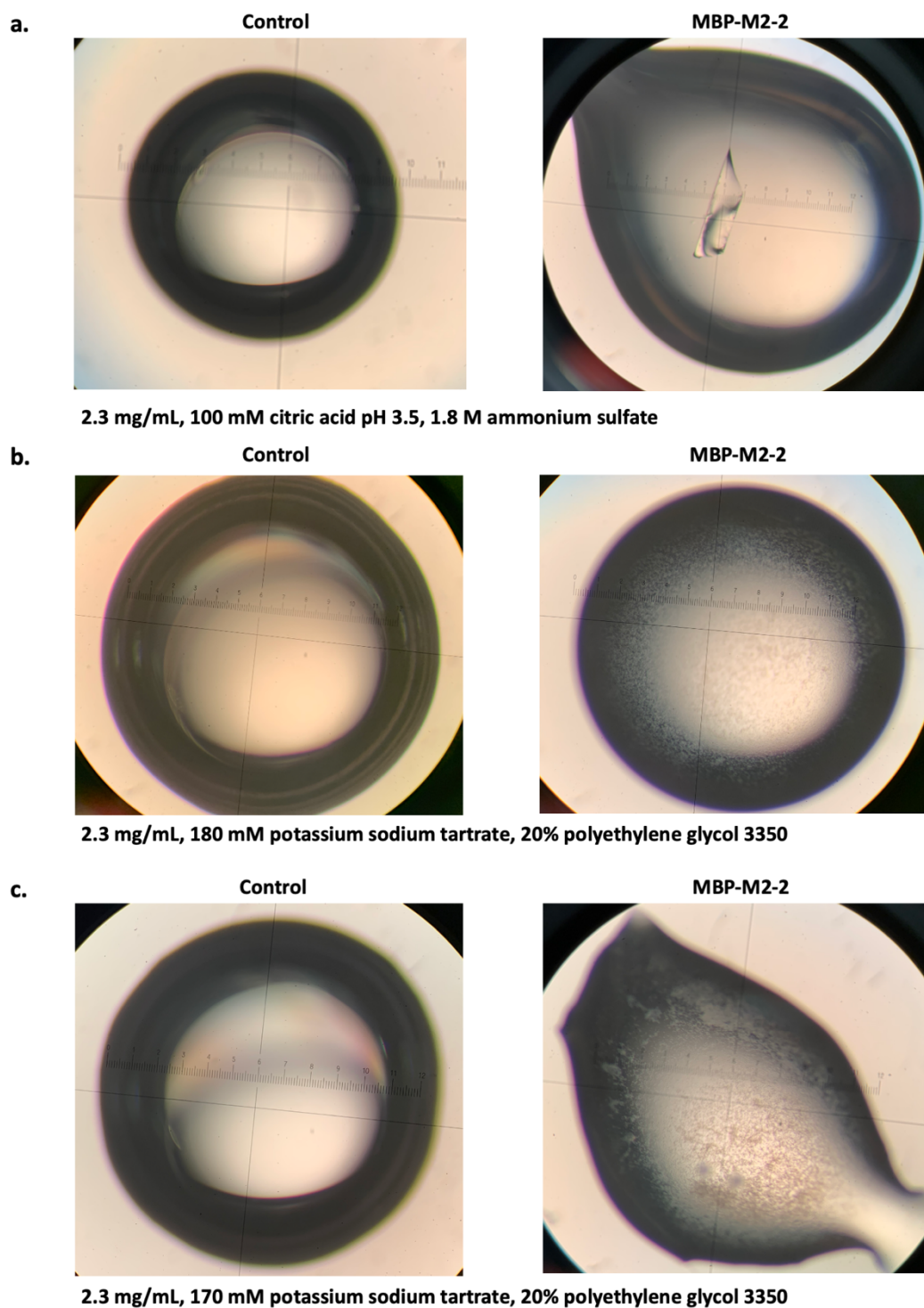


**Figure 6. MBP-M2-2 Crystal Optimization Experiments.** MBP-M2-2 was concentrated to 2.3 mg/mL and was tested under 21 hanging-drop conditions based on previous screening results (Figure 5).

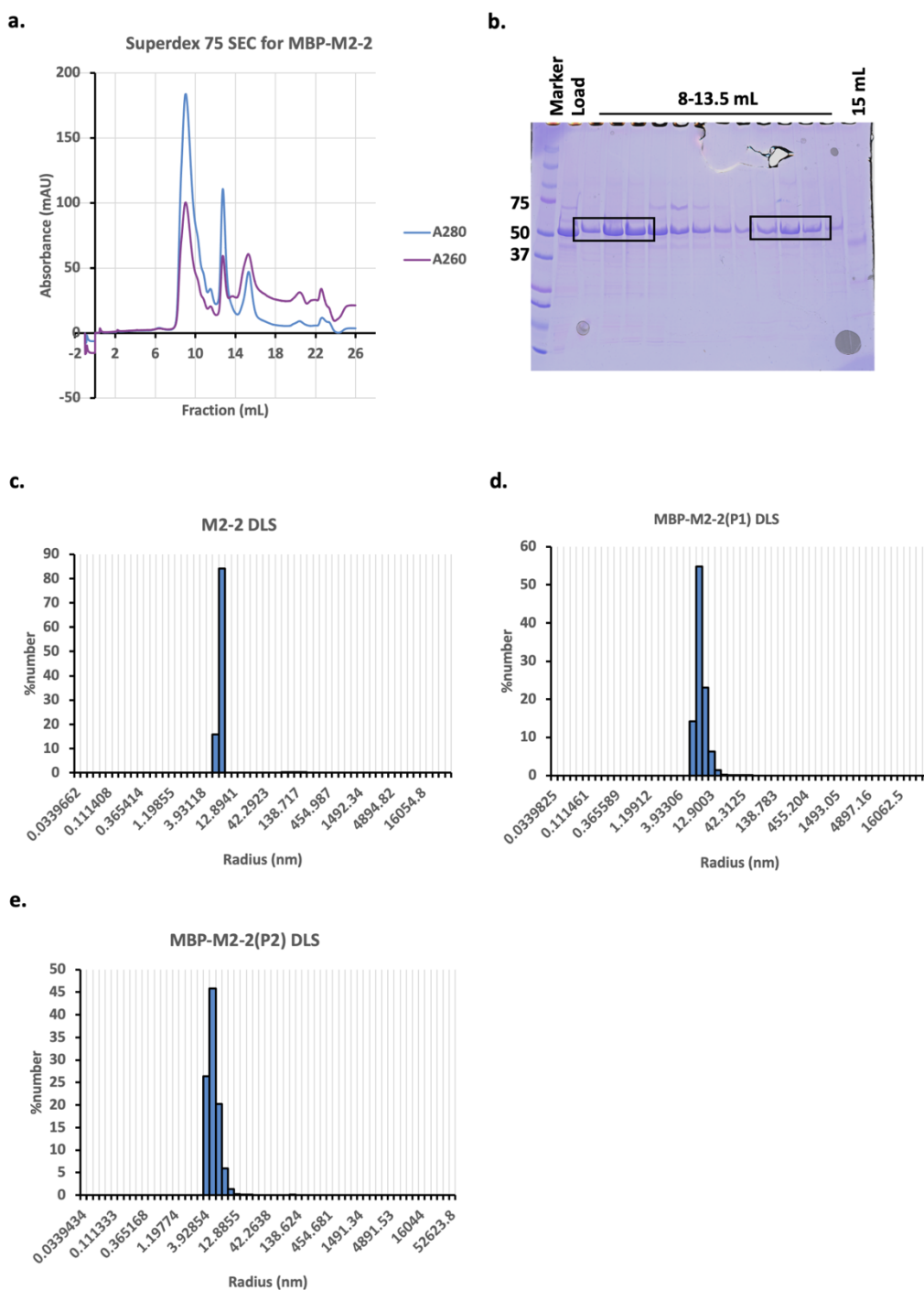


**Figure 7. DLS Analysis of M2-2, MBP-M2-2<sub>P1</sub>, and MBP-M2-2<sub>P2</sub>.** **a** MBP-M2-2 was purified as described previously and then eluted from a Superdex 75 column. Two peaks were eluted from the column between 8-11.5 mL and 12-15 mL. **b** The fractions were run on SDS-PAGE. Samples from the first peak were saved as MBP-M2-2<sub>P1</sub> while fractions from the second, MBP-M2-2<sub>P2</sub>, were also saved. **c** DLS shows that 99.9% of particles have a radius of approximately 7 nm. **d** MBP-M2-2<sub>P1</sub> particles had an average radius of 8.7 nm. **e** MBP-M2-2<sub>P2</sub> particles had an average radius of 5.2 nm.

an FEI Talos 120 kV TEM (Emory IEMC), revealing M2-2 particles that are about 10 nm in diameter (Figure 8a) and MBP-M2-2<sub>p1</sub> particles that are 25 nm in diameter (Figure 8b). The findings suggest that M2-2 and MBP-M2-2 are able to form oligomer complexes in solution.

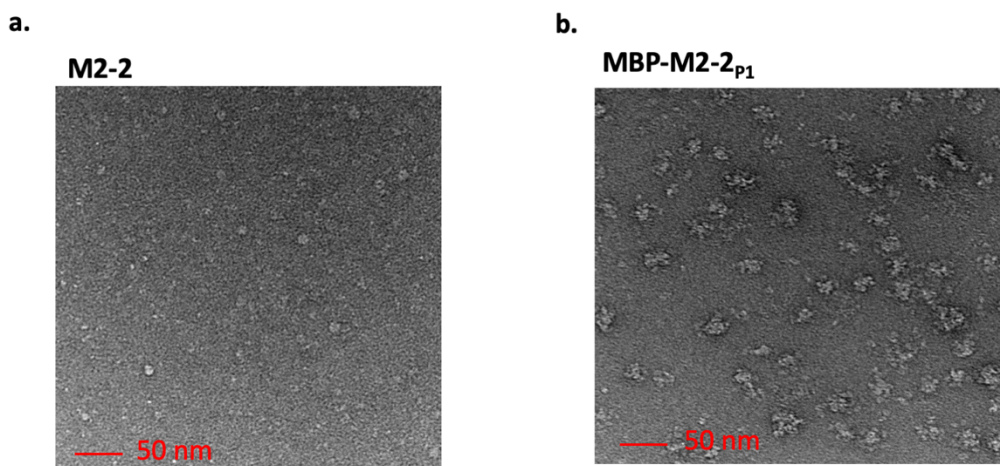


**Figure 8. Negative Stain EM of M2-2 and MBP-M2-2<sub>p1</sub>.** M2-2 and MBP-M2-2<sub>p1</sub> samples were loaded onto an EM grid, stained with uranyl formate, and imaged under an electron microscope. M2-2 forms particles with a diameter of 10 nm while MBP-M2-2<sub>p1</sub> forms particles that are 25 nm in diameter.

## METHODS AND MATERIALS

### *E. coli* Transformation and MBP-M2-2 Expression

The M2-2 gene was obtained from the hRSV A2 strain. The pET expression vector was synthesized by Synbio Technologies to include a TEV protease recognition site, MBP, and a 6x-histidine tag fused with M2-2. Expression was placed under the control of a T7 promoter and the *lac* operator. The plasmid also contains the *lacI* gene encoding for the *lac* repressor and a kanamycin resistance gene.

BL21(DE3) competent cells were used for transformation and expression of M2-2. 100  $\mu$ L of cells were mixed with 50 ng of plasmid, and the mixture was allowed to settle on ice for

30 minutes. The cells were then heat shocked in a 42°C water bath for 60 seconds and then placed on ice for 3 minutes to allow the cells to recover. The cells were then mixed with 900 µL of LB media and incubated at 37°C for one hour while shaking at 220 rpm. The cells were centrifuged at 2000 rpm for 3 minutes, and 900 µL of supernatant was discarded. Afterward, the cells were resuspended and plated on an LB agar plate with kanamycin (0.05 mg/mL). The plate was then incubated at 37°C for 16 hours.

A single colony was selected and grown in 200 mL LB containing kanamycin at 0.05 mg/mL at 37°C overnight. 10 mL of culture was then added to 1 L of LB containing kanamycin, and the process was repeated to produce 12 L of cells. The cells were incubated at 37°C until they reached an OD600 between 0.6 and 0.8. Flasks were then placed in an ice bath to stop cell growth, and IPTG was added to a concentration of 1 mM in order to induce MBP-M2-2 expression. The cells were then left at 16°C while shaking at 220 rpm overnight for protein expression. Finally, cells were harvested by centrifugation at 3800 rpm for 30 minutes and then stored at -80°C.

### **MBP-M2-2 Purification**

Cells were resuspended in lysis buffer containing 30 mM Tris-HCl pH 8.0, 300 mM NaCl, 20 mM imidazole with 1 mM PMSF, pepstatin (1 µL/mL), leupeptin (1 µL/mL), and aprotinin (1 µL/mL) protease inhibitors. The cells were then sonicated at 50% amplitude for a total of 12 minutes with 3 seconds pulses followed by 3 seconds off. The lysate was then centrifuged at 18,000 rpm for 45 minutes, and the supernatant was incubated with Ni-NTA resin at 4°C overnight. After incubation, the sample and resin were loaded on a gravity column, and the

flowthrough was collected. Then, the column was washed with 20 mM and 100 mM imidazole before eluting the protein with 200 mM and 1 M imidazole.

The elution fractions were then combined, placed in 25 kDa dialysis bags, and left in 2 L of 30 mM Tris-HCl pH 8.0, 50 mM NaCl to remove the imidazole and reduce the salt concentration. After 17 hours at 4°C, the bags were transferred to a new 1 L of buffer for another four hours to continue buffer exchange. The sample was then loaded on a 5 mL HiTrap Capto Q ImprRes column (Cytiva Life Sciences) using a Rainin Dynamax peristaltic pump. The column was then loaded on an AKTA Pure system where the column was washed with 10 mL of 30 mM Tris-HCl pH 8.0, 50 mM NaCl followed by an increasing salt gradient up to 1 M NaCl. During purification, the NaCl concentration was occasionally held constant to thoroughly elute protein and to separate peaks.

Finally, the eluted fractions were concentrated to 2 mL and loaded onto a Superdex 200 Increase 10/300 GL column (Cytiva Life Sciences) using a 2 mL capillary loop on the AKTA Pure system. The column was then eluted with 30 mM Tris-HCl pH 8.0, 150 mM NaCl. The fractions were frozen in liquid nitrogen and stored at -80°C.

## **M2-2 Purification**

Cells were sonicated and purified by nickel affinity chromatography as described previously for MBP-M2-2. Afterward, TEV protease was added at a 1:20 TEV-to-MBP-M2-2 mass ratio, and the mixture was placed in a 1 kDa dialysis bag. The sample was then left in 1 L of 30 mM Tris-HCl pH 8.0, 300 mM NaCl, 2 mM BME for 13 hours and later transferred to 1 L of 30 mM Tris-HCl pH 8.0, 50 mM NaCl for four hours. The cleaved protein was then loaded onto a

second nickel column, and the flowthrough was collected and reloaded onto the column to maximize binding. Then, the column was washed with 20 mM imidazole and eluted with 1 M imidazole.

The sample was then purified by anion exchange chromatography as described previously. It was then loaded on a final nickel column, washed with 0 mM imidazole, and eluted with 100 mM and 1 M imidazole. Finally, the sample was purified by SEC as described previously.

### **Crystal Screening and Optimization**

Pure MBP-M2-2 was concentrated to 9.93 mg/mL and tested on a pre-crystallization test (Hampton Research). The protein was then tested in 768 conditions using Crystal Screen, Index HT, GRAS 1-4 (Hampton Research), and Wizard 1-4 (Rigaku Corporation) screening kits. A Crystal Phoenix (Art Robbins Instruments) set up drops of 0.2  $\mu$ L protein and 0.2  $\mu$ L buffer with 60  $\mu$ L buffer reservoirs on 96-well 3-drop plates. The drops were then incubated at 30°C and imaged with a Formulatrix RockImager-1000 under visible and UV light.

Buffer conditions that produced microcrystals were identified and modified to optimize crystal growth. The concentration of each salt and precipitant was decreased by 10%, 15%, or 20%. From the three original buffer conditions, an additional seven conditions were created, producing 21 total conditions to be tested. The MBP-M2-2 sample was concentrated to 2.3 mg/mL and tested again on a pre-crystallization test before setting up hanging-drop wells. Each well was filled with 500  $\mu$ L of buffer. Each 2  $\mu$ L drop of protein was mixed with 2  $\mu$ L of buffer on

glass cover slides which were then inverted and sealed above each well. The tray was incubated at 30°C and observed to identify crystal growth.

### **Dynamic Light Scattering**

The M2-2, MBP-M2-2<sub>P1</sub>, and MBP-M2-2<sub>P2</sub> samples were concentrated to 0.3 mg/mL, 2.3 mg/mL, and 1.5 mg/mL respectively and centrifuged at 14,800 rpm for 10 minutes to remove any precipitation. They were then loaded on a 384-well plate which was centrifuged for 10 minutes at 3,800 rpm to remove air bubbles that may interfere with the reading. The plate was then loaded into a DynaPro Plate Reader III (Wyatt Technology), where a total of 10 two-second acquisitions were taken of the sample.

### **Negative Stain Electron Microscopy**

EM grids were first glow discharged in a Pelco Glow Discharger. Purified samples of M2-2, MBP-M2-2<sub>P1</sub>, and MBP-M2-2<sub>P2</sub> were diluted to a concentration of 0.025 mg/mL, and 3 µL of the sample was applied to each grid for one minute. The grids were then blotted, washed in ddH<sub>2</sub>O, blotted again, and then washed in ddH<sub>2</sub>O and blotted a second time. Afterward, the grids were stained in 0.75% uranyl formate for 10 seconds, blotted, and stained again in uranyl formate for one minute. Finally, the grids were blotted and left to dry. The grids were then loaded and imaged under an the FEI Talos 120 KV TEM at Emory IEMC.

## DISCUSSION AND FUTURE DIRECTIONS

As there is currently no reported structural information on M2-2, we were able to address this knowledge gap by reporting the expression and purification of M2-2 and MBP-M2-2. We also showed crystallization of MBP-M2-2 along with negative stain EM images depicting the proteins as oligomers. However, further optimization must be done to obtain pure protein and crystals to solve the structure of M2-2.

The expression and purification of MBP-M2-2 have been successfully optimized for large-scale expression and purification. However, we were unable to reliably purify M2-2 in sufficient quantities for crystallization experiments. Our current purification protocol was able to produce pure protein, but it came at the cost of significant yield (Figure 4e-f). One source of protein loss was due to incomplete TEV protease digestion, as not all MBP-M2-2 is successfully cleaved to M2-2 (Figure 4a). We conducted several experiments to improve TEV protease efficiency by altering the sample conditions. These conditions included increasing the incubation time, lowering the NaCl concentration, replacing BME as a reducing agent with dithiothreitol (DTT), and increasing the TEV-to-M2-2 ratio. However, these conditions did not appear to improve digestion efficiency significantly (Supplemental Figure 1). In addition, because some protein is lost after each step in purification, the repeated chromatography cycles amplified M2-2 loss. This is especially true for anion exchange chromatography, where protein was lost without efficient purification (Figure 4b-c). To combat this, we attempted to avoid excess purification steps and directly purify the sample on SEC after TEV digestion (Supplemental Figure 2b-c). We also attempted to incubate the sample in 1 M NaCl after TEV digestion and then purify it over Ni-NTA to prevent any ionic interactions between MBP and

M2-2 (Supplemental Figure 2d). Regardless, neither of these attempts showed significant improvement.

Further attempts to optimize M2-2 purification failed to separate M2-2 from MBP and MBP-tagged M2-2. This could be due to the tendency for M2-2 to form oligomers that keep it bound to MBP-M2-2. In addition, it may have an affinity for MBP, keeping M2-2 bound even after TEV digestion. To work around this issue, we have subcloned 10x-histidine-tagged M2-2 without MBP into a pET expression vector (Supplemental Figure 4). This allows us to avoid needing to separate MBP from M2-2 after TEV cleavage, coming at the cost of losing the solubility offered by MBP.

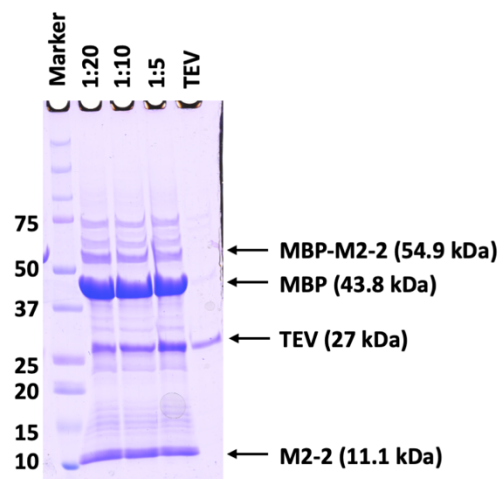
We also crystallized MBP-M2-2 successfully, though additional optimization is required. Solving the crystal structure of MBP-M2-2 would provide valuable insight into the structure of M2-2 and can serve as an alternative to solving the structure of M2-2 alone. Crystallization chaperones have often been used when reporting structures, and MBP is among the most popular of these chaperones (Jin et al. 2017). A new helical linker design connecting MBP with M2-2 could further increase the likelihood of crystallization (Jin et al. 2017). While several conditions appear to allow microcrystal growth, testing additional conditions could increase the likelihood of forming crystals. In addition, many promising conditions included the precipitant PEG 3350. As a result, an additional crystal screening kit using PEG could offer other potential crystallization conditions.

DLS results showed that the radius of MBP-M2-2<sub>P1</sub> was larger than the radius of MBP-M2-2<sub>P2</sub>, which corroborates the SEC data. We also used negative stain EM to characterize M2-2 and M2-2<sub>P1</sub> and identified 10 nm and 25 nm particles for the two samples respectively. These

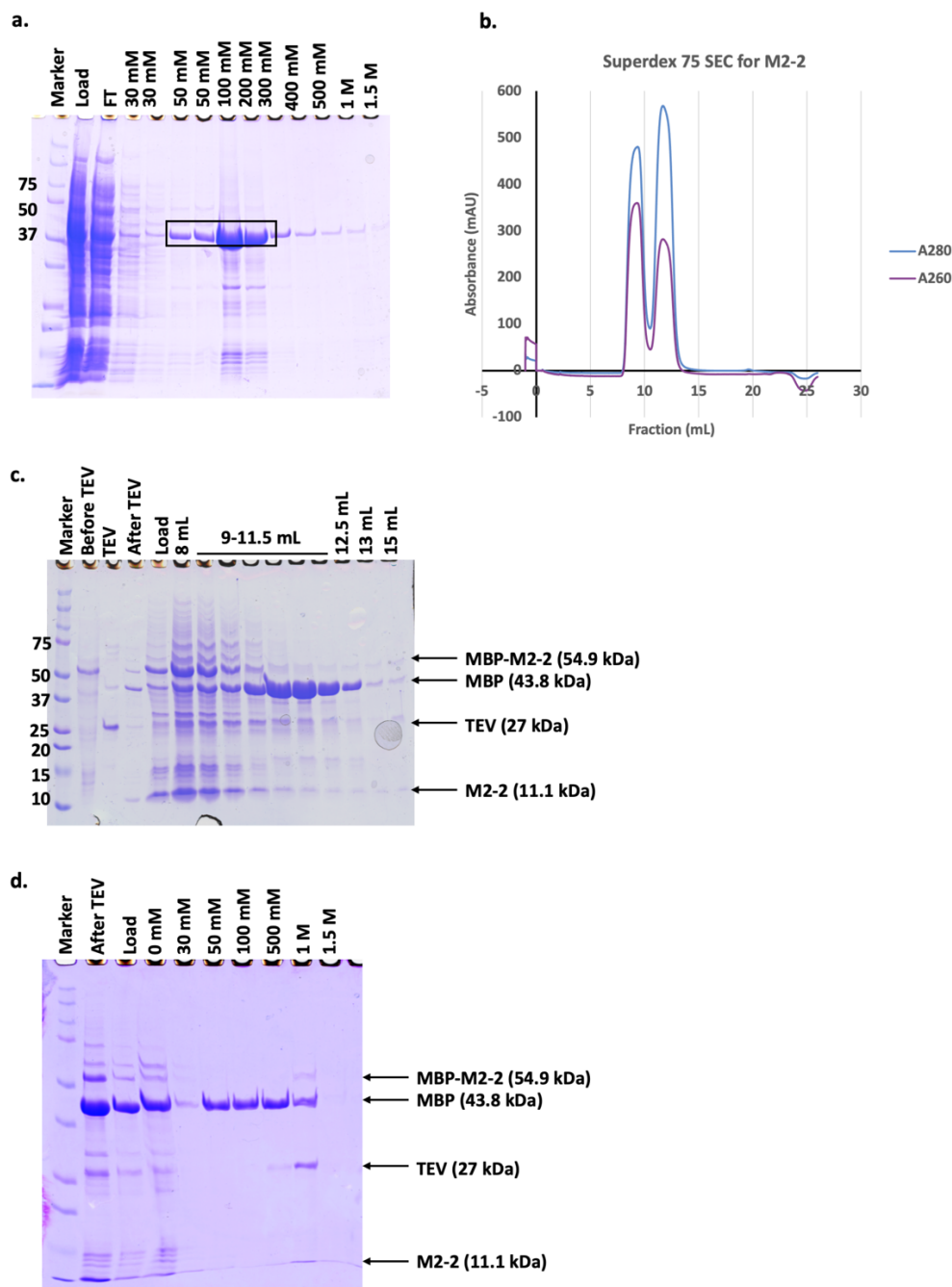
large particles likely indicate that M2-2 and MBP-M2-2 form oligomers in solution given M2-2 is approximately 3 nm based on its comparison with the reported M2-1 (Gao et al. 2020). The large size of MBP-M2-2 particles most likely contributed to the difficulty in forming full crystals. However, we found that these proteins do not form monomers like we expected, opening the possibility of using cryo-electron microscopy instead of X-ray crystallography.

Pull-down assays of MBP-M2-2 mixed with untagged M2-2 can be done in the future to confirm the interactions between M2-2 monomers. Another goal is the expression and purification of 10x-histidine-tagged M2-2 which has already been successfully subcloned in an expression vector. With the knowledge that M2-2 forms large particles in solution, we can attempt to solve the structure without the need for high-yield purification and optimized crystallization. Cryo-EM can allow us to solve the structure of M2-2 and provide the first structure of the protein, opening the door to understanding M2-2 at a biochemical level and allowing us to better understand RNA synthesis in NNS viruses.

## SUPPLEMENTARY FIGURES



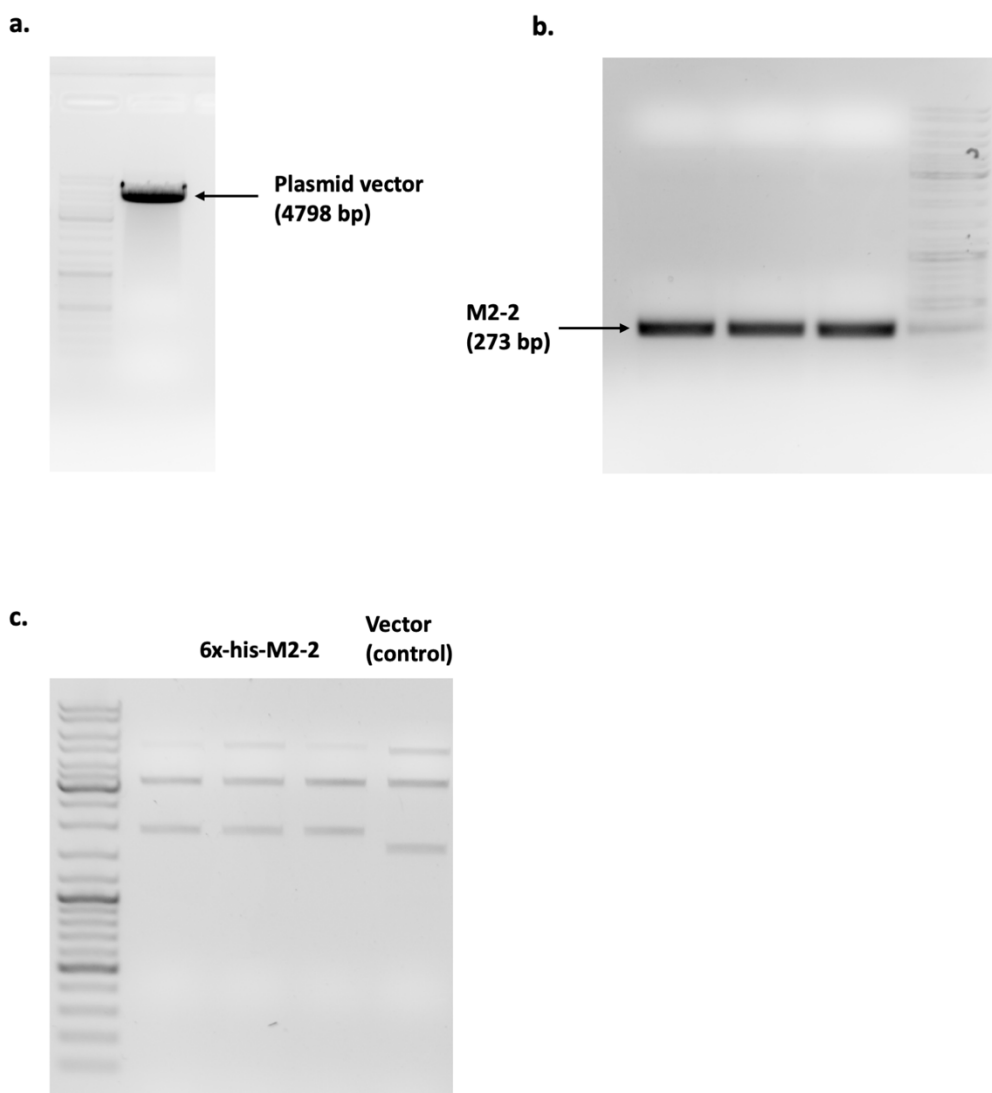
**Supplementary Figure 1. TEV Protease Digestion Experiment.** MBP-M2-2 was purified by Ni-NTA. Equal volumes of MBP-M2-2 were mixed with TEV in a TEV-to-MBP-M2-2 mass ratio of 1:20, 1:10, and 1:5. Digestion occurred overnight at 4°C in 30 mM Tris-HCl pH 8.0, 300 mM NaCl, 10 mM maltose.



**Supplemental Figure 2. M2-2 Purification Optimization Experiment.** Due to low M2-2 yield, we attempted to optimize the purification process. **a** M2-2 was purified over Ni-NTA as described previously with 30 mM Tris-HCl pH 8.0, 300 mM NaCl, 10 mM maltose, and imidazole. **b** To avoid loss of M2-2 through extra purification cycles, we directly purified the sample after TEV digestion on a Superdex 75 Increase 10/300 GL column. Two peaks appeared with eluted protein (8-10.5 mL and 11-13 mL). **c** SEC fractions were analyzed by SDS-PAGE. **d** M2-2 was incubated with 1 M NaCl to prevent ionic interactions between MBP and M2-2. It was then purified over Ni-NTA and eluted with imidazole.

Condition #	Citric acid pH 3.5 (mM)	Ammonium sulfate (M)
1	100	2
2	90	2
3	85	2
4	80	2
5	100	1.8
6	100	1.7
7	100	1.6
Condition #	Potassium sodium tartrate tetrahydrate (mM)	Polyethylene glycol 3350 (%)
8	200	20%
9	180	20%
10	170	20%
11	160	20%
12	200	18%
13	200	17%
14	200	16%
Condition #	Sodium malonate pH 7.0 (mM)	Polyethylene glycol 3350 (%)
15	200	20%
16	180	20%
17	170	20%
18	160	20%
19	200	18%
20	200	17%
21	200	16%

**Supplemental Figure 3. Crystal Optimization Conditions.** Crystal screening revealed three buffer conditions that produced microcrystals. The composition of each buffer was decreased by 10%, 15%, and 20% to determine the optimal condition for crystal growth.



**Supplementary Figure 4. M2-2 Subcloning.** The MBP-M2-2 expression plasmid was subcloned to create a 10x-histidine-tagged M2-2 plasmid. **a** TOP10 *E. coli* cells were transformed with the expression vector and grown before lysing and purifying the DNA using Miniprep. **b** PCR amplified the M2-2 gene with TAQ polymerase using the MBP-M2-2 plasmid as a template. **c** The vector and gene were treated with T4 polymerase and then annealed. The plasmid was then used to transform TOP10 competent cells. The new plasmid was obtained through Miniprep and treated with the AseI restriction enzyme to confirm successful cloning.

**REFERENCES**

- Asenjo, A., and N. Villanueva. "Phosphorylation of the Human Respiratory Syncytial Virus P Protein Mediates M2-2 Regulation of Viral Rna Synthesis, a Process That Involves Two P Proteins." *Virus Res* 211 (Jan 4 2016): 117-25.  
<https://doi.org/10.1016/j.virusres.2015.10.011>.  
<https://www.ncbi.nlm.nih.gov/pubmed/26474524>.
- Battles, M. B., and J. S. McLellan. "Respiratory Syncytial Virus Entry and How to Block It." *Nat Rev Microbiol* 17, no. 4 (Apr 2019): 233-45. <https://doi.org/10.1038/s41579-019-0149-x>.  
<https://www.ncbi.nlm.nih.gov/pubmed/30723301>.
- Bermingham, A.; Collins, Peter L. "The M2–2 Protein of Human Respiratory Syncytial Virus Is a Regulatory Factor Involved in the Balance between Rna Replication and Transcription." *Biochemistry* 96, no. 20 (September 28, 1999): 11259–64.  
<https://doi.org/10.1073/pnas.96.20.11259>.
- Blanchard, E. L., M. R. Braun, A. W. Lifland, B. Ludeke, S. L. Noton, D. Vanover, C. Zurla, R. Fearn, and P. J. Santangelo. "Polymerase-Tagged Respiratory Syncytial Virus Reveals a Dynamic Rearrangement of the Ribonucleocapsid Complex During Infection." *PLoS Pathog* 16, no. 10 (Oct 2020): e1008987. <https://doi.org/10.1371/journal.ppat.1008987>.  
<https://www.ncbi.nlm.nih.gov/pubmed/33031461>.
- Boyoglu-Barnum, S., T. Chirkova, and L. J. Anderson. "Biology of Infection and Disease Pathogenesis to Guide Rsv Vaccine Development." *Front Immunol* 10 (2019): 1675.  
<https://doi.org/10.3389/fimmu.2019.01675>.  
<https://www.ncbi.nlm.nih.gov/pubmed/31402910>.

- Cheng, X., H. Park, H. Zhou, and H. Jin. "Overexpression of the M2-2 Protein of Respiratory Syncytial Virus Inhibits Viral Replication." *J Virol* 79, no. 22 (Nov 2005): 13943-52.  
<https://doi.org/10.1128/JVI.79.22.13943-13952.2005>.  
<https://www.ncbi.nlm.nih.gov/pubmed/16254330>.
- Collins, P. L., R. Fearn, and B. S. Graham. "Respiratory Syncytial Virus: Virology, Reverse Genetics, and Pathogenesis of Disease." *Curr Top Microbiol Immunol* 372 (2013): 3-38.  
[https://doi.org/10.1007/978-3-642-38919-1\\_1](https://doi.org/10.1007/978-3-642-38919-1_1).  
<https://www.ncbi.nlm.nih.gov/pubmed/24362682>.
- Gao, Y., D. Cao, S. Pawnikar, K. P. John, H. M. Ahn, S. Hill, J. M. Ha, *et al.* "Structure of the Human Respiratory Syncytial Virus M2-1 Protein in Complex with a Short Positive-Sense Gene-End Rna." *Structure* 28, no. 9 (Sep 1 2020): 979-90 e4.  
<https://doi.org/10.1016/j.str.2020.07.001>.  
<https://www.ncbi.nlm.nih.gov/pubmed/32697936>.
- Griffiths, Cameron, Steven J. Drews, and David J. Marchant. "Respiratory Syncytial Virus: Infection, Detection, and New Options for Prevention and Treatment." *Clinical Microbiology Reviews* 30, no. 1 (2017): 277-319. <https://doi.org/10.1128/cmr.00010-16>.
- Jin, Hong; Cheng, Xing; Zhou, Helen Z.; Li, Shenqiang; Seddiqui, Adam. "Respiratory Syncytial Virus That Lacks Open Reading Frame 2 of the M2 Gene (M2-2) Has Altered Growth Characteristics and Is Attenuated in Rodents." *Journal of Virology* 74, no. 1 (2000): 74-82. <https://doi.org/10.1128/jvi.74.1.74-82.2000>.
- Jin, T., W. Chuenchor, J. Jiang, J. Cheng, Y. Li, K. Fang, M. Huang, P. Smith, and T. S. Xiao. "Design of an Expression System to Enhance Mbp-Mediated Crystallization." *Sci Rep* 7 (Jan 23

2017): 40991. <https://doi.org/10.1038/srep40991>.

<https://www.ncbi.nlm.nih.gov/pubmed/28112203>.

Nikolic, J., R. Le Bars, Z. Lama, N. Scrima, C. Lagaudriere-Gesbert, Y. Gaudin, and D. Blondel.

"Negri Bodies Are Viral Factories with Properties of Liquid Organelles." *Nat Commun* 8, no. 1 (Jul 5 2017): 58. <https://doi.org/10.1038/s41467-017-00102-9>.

<https://www.ncbi.nlm.nih.gov/pubmed/28680096>.

Rincheval, V., M. Lelek, E. Gault, C. Bouillier, D. Sitterlin, S. Blouquit-Laye, M. Galloux, *et al.*

"Functional Organization of Cytoplasmic Inclusion Bodies in Cells Infected by Respiratory Syncytial Virus." *Nat Commun* 8, no. 1 (Sep 15 2017): 563.

<https://doi.org/10.1038/s41467-017-00655-9>.

<https://www.ncbi.nlm.nih.gov/pubmed/28916773>.

Scudero, Orlando Bonito, Verônica Feijoli Santiago, Giuseppe Palmisano, Fernando Moreira

Simabuco, and Armando Morais Ventura. "The Respiratory Syncytial Virus M2-2 Protein Is Targeted for Proteasome Degradation and Inhibits Translation and Stress Granules Assembly." (Preprint, submitted in 2023). <https://doi.org/10.1101/2023.01.02.522538>.

<https://www.biorxiv.org/content/10.1101/2023.01.02.522538v1.full>.

Simões, E. A. F., Kimberly J. Center, Alan T. N. Tita, Kena A. Swanson, David Radley, John

Houghton, Stephanie B. McGrory, *et al.* "Prefusion F Protein–Based Respiratory Syncytial Virus Immunization in Pregnancy." *New England Journal of Medicine* 386 (2022): 1615-26. <https://doi.org/10.1056/NEJMoa2106062>.

Teng, M. N.; Whitehead, S. S.; Bermingham, A., St Claire, M.; Elkins, W. R.; Murphy, B. R.;

Collins, P. L. "Recombinant Respiratory Syncytial Virus That Does Not Express the Ns1 or

M2-2 Protein Is Highly Attenuated and Immunogenic in Chimpanzees." *Journal of Virology* 74, no. 19 (2000): 9317-21. <https://doi.org/10.1128/jvi.74.19.9317-9321.2000>.